

Experimental studies of a thermoacoustic Stirling prime mover and its application to a cooler

Y. Ueda,^{a)} T. Biwa, and U. Mizutani

Department of Crystalline Materials Science, Nagoya University, Nagoya 464-8603, Japan

T. Yazaki

Department of Physics, Aichi University, Kariya 448, Japan

(Received 15 August 2003; revised 19 December 2003; accepted 28 December 2003)

An acoustic field spontaneously induced in a thermoacoustic prime mover consisting of a looped tube and resonator is determined through simultaneously measurements of pressure P and velocity U . A thermal efficiency of the thermoacoustic prime mover of this type has been reported to reach 30%. The measurements of the acoustic field in the present system revealed that a phase lead of U relative to P takes a negative value of about -20° in the regenerator where the output power of the prime mover is generated. It was concluded that the possession of a negative phase lead at this position is taken as a clue in a significant increase in the output power. Moreover, the analysis in the thermoacoustic mechanism shows that a precise position for the location of a second regenerator acting as a heat pump exists in the looped tube. Indeed, by locating the second regenerator at the position, a thermoacoustic cooler was constructed. The thermoacoustic cooler could generate a low temperature of -25°C without involving any moving parts. © 2004 Acoustical Society of America. [DOI: 10.1121/1.1649333]

PACS numbers: 43.35.Ud [RR]

Pages: 1134–1141

I. INTRODUCTION

A conventional internal-combustion prime mover such as a car engine has many mechanical parts like pistons, valves, etc. An efficient energy conversion can be achieved, only if these mechanical parts are properly tuned. This requires high maintenance- and production costs. On the other hand, a thermoacoustic prime mover can perform an efficient energy conversion without nuisance mechanical parts.

A thermoacoustic prime mover is composed of a regenerator, two heat exchangers, and a tube. Here, the regenerator is sandwiched by the heat exchangers in the tube. When a steep temperature gradient is set up along the regenerator by the heat exchangers, an acoustic wave accompanying pressure

$$P = p e^{i\omega t}, \quad (1)$$

and cross-sectional mean velocity

$$U = u e^{i(\omega t + \Phi)}, \quad (2)$$

is spontaneously generated in the tube, where ω is an angular frequency and Φ is a phase lead of U relative to P . The spontaneously generated acoustic wave forces a gas parcel in the regenerator to experience a thermodynamic cycle consisting of the compression, heating, expansion, and cooling. As a result, the energy conversion of heat flow Q into work flow I occurs without involving moving parts.^{1–4}

Thermoacoustic prime movers are classified into two types depending on the value of the phase lead Φ ; one is a standing wave thermoacoustic prime mover and the other is a traveling wave one. In a standing wave prime mover, a gas parcel with Φ nearly equal to $\pi/2$ contributes to the energy

conversion through irreversible thermal contacts with wall in a regenerator. We call this phase lead ($\Phi = \pi/2$) the *standing wave phase*. Many prime movers of this type have been constructed^{5,6} and used for operating a refrigerator to liquefy natural gas.⁷ However, their thermal efficiencies are at best⁸ 20% because their energy conversion is based on the irreversibility.¹

A traveling wave thermoacoustic prime mover was originally proposed by Ceperley in 1979.⁹ In this prime mover, a gas parcel with Φ nearly equal to zero contributes to the energy conversion through reversible thermal contacts with wall in a regenerator. This phase lead ($\Phi = 0$) is called the *traveling wave phase*. In order to gain a deeper insight into details of a thermodynamic cycle performed in the traveling wave prime mover, we attempt to elucidate the relation between pressure P and cross-sectional mean displacement ζ under the condition $\Phi = 0$. This is illustrated in Fig. 1(a). Since ζ is always out of phase with the velocity U by $\pi/2$, it is also out of phase with P by $\pi/2$. When a gas parcel with $\Phi = 0$ locally makes isothermal contacts with wall in a regenerator, where a finite temperature gradient exists as shown in Fig. 1(b), it would undergo the thermodynamic cycle of four stages: (1) the gas parcel is pressurized around the cold end (compression); (2) moves to the hot end (heating); (3) is depressurized around the hot end (expansion); and (4) moves back to the cold end (cooling). Ceperley pointed out that this thermodynamic cycle is essentially the same as that performed in a conventional Stirling prime mover. Since a conventional Stirling prime mover has a thermal efficiency of 20%–38%,¹⁰ he considered that a traveling wave thermoacoustic prime mover can in principle have a high efficiency without any moving parts. However, it had not been realized until 1998, when Yazaki *et al.* succeeded for the first time in constructing a traveling wave thermoacoustic prime mover by using a looped tube.¹¹ Yazaki *et al.*

^{a)}Electronic mail: ueda@mizu.xtal.nagoya-u.ac.jp

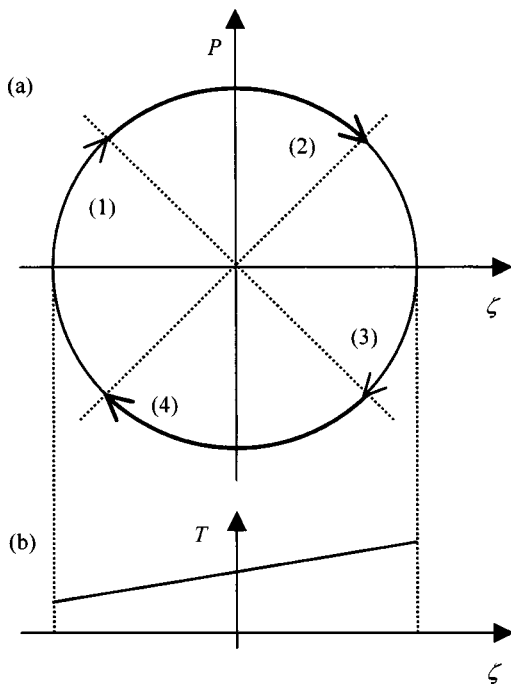


FIG. 1. (a) Relation between pressure P and displacement ζ with the traveling wave phase. (b) Temperature gradient in a regenerator.

simultaneously measured both P and U in the acoustic field induced in the looped tube prime mover, and found that its phase lead Φ was close to a traveling wave phase ($\Phi = 0$) in the regenerator.

In 1999, Backhaus and Swift upgraded a thermal efficiency up to 30% by introducing a resonator in a looped tube.⁸ The efficiency has reached a level comparable to that of a car engine.¹⁰ They attribute such a high efficiency to the fulfillment of the two conditions. One is the possession of the traveling wave phase and the other is that of a high value of a dimensionless acoustic impedance z defined as

$$z = \frac{P/P_m}{U/c}, \quad (3)$$

where P_m is a mean pressure and c is the adiabatic sound speed. If a free-traveling acoustic wave, whose Φ is always zero, is generated in a thermoacoustic prime mover, the acoustic impedance z would be fixed at the specific heat ratio $\gamma = c_p/c_v$, where c_p and c_v are specific heat of the gas at constant pressure and volume, respectively. The low value of z ($=\gamma$) would lead to significant viscous losses in a regenerator because of the motion of the gas with a high velocity. In order to reduce the viscous losses, z should be increased far beyond the value of γ . Though they stressed the importance of these two conditions above to achieve a high efficiency, the values of Φ and z in their prime mover have not been experimentally determined.

This paper describes an attempt in the optimization of the feature size of the Backhaus and Swift-style thermoacoustic prime mover so as to generate an intense acoustic wave, and presents the values of Φ and z determined by simultaneous measurements of P and U in the prime mover. Their preliminary data were already reported.¹² We show from the present data that the energy conversion from heat

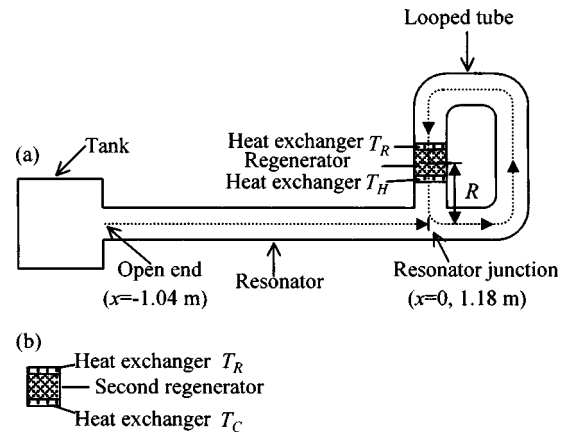


FIG. 2. (a) Thermoacoustic Stirling prime mover consisting of a looped tube and a resonator. A regenerator sandwiched by two heat exchangers is located in the looped tube. (b) Regenerator working as a thermoacoustic heat pump. Two heat exchangers are located on its both ends.

flow Q into work flow I is performed in the regenerator by a gas parcel having an acoustic impedance large enough to suppress viscous losses. Its phase lead Φ , however, turns out to be negative rather than zero corresponding to a pure traveling wave phase. We demonstrate below that the possession of a negative value of the phase lead in a regenerator plays a key role in producing the output power of the present prime mover.

In the second part of the present work, a construction of a thermoacoustic Stirling cooler driven by the present prime mover is reported. The experimental results obtained from the simultaneous measurements of P and U allow us to pinpoint the position where the reversed Stirling cycle can be executed. Indeed, by locating a second regenerator acting as a heat pump at this particular position, we could construct the cooler without involving any moving parts. It could generate -25°C and have a cooling power of 11 W at 0°C when an input heat power was 210 W.

II. THERMOACOUSTIC STIRLING PRIME MOVER

A. Apparatus

The present thermoacoustic prime mover, as schematically illustrated in Fig. 2(a), is composed of a looped tube and resonator made of Pyrex glass tubes. They are 40 mm in inner diameter and are filled with atmospheric air. One end of the resonator, which is hereafter referred to as the resonator junction, is joined with the looped tube. The other end, called the open end of the resonator, is connected to a $2.0 \times 10^{-2}\text{-m}^3$ tank. Pressure transducers are installed on the wall of both looped tube and resonator. The direction of gravity is headed from upper to lower sides in Fig. 2(a).

A regenerator of 35 mm in length is made of a stack of 60-mesh stainless-steel screens with a wire diameter of 0.12 mm and is located in the looped tube, as shown in Fig. 2(a). From the measurement of porosity of the regenerator, we estimated its hydraulic radius¹³ to be 0.13 mm. This is much smaller than the thermal penetration depth¹⁴ δ_t formed at the wall and, thus, we consider that a good thermal contact between a gas parcel and wall of the screens is ensured throughout the present work. The two heat exchangers,

where brass plates 0.5 mm in thickness and 10 mm in height are placed at 0.5-mm intervals, are located on both sides of the regenerator. One is water-cooled and kept at room temperature T_R . The other is heated by an electrical resistance heater wound around it, and its temperature T_H is controlled by the heater power Q_H up to 210 W.

B. Optimization to generate an intense acoustic wave

The performance of the present apparatus was tested by varying the total length of the looped tube L_l , the length of the resonator L_r , and the distance R from the resonator junction to the center of the regenerator [see Fig. 2(a)]. When Q_H exceeded some critical value Q_{cri} , a gas oscillation spontaneously generated in the setup with all combinations of L_l , L_r , and R we tested. The wavelength λ of the acoustic wave thus generated was estimated from its frequency, and it was found that λ is essentially four times as long as the sum of L_l and L_r . Hence, we call the acoustic oscillation the quarter-wavelength mode, which is the same as that induced in the Backhaus and Swift prime mover.⁸ As Q_H was increased beyond Q_{cri} , the amplitude of the acoustic oscillation was also increased. We measured the position dependence of the pressure amplitude when $Q_H=210$ W. It was found that the pressure node and antinode always appear near the open end of the resonator and the cold end of the regenerator, respectively, regardless of the combinations of L_l , L_r , and R . However, the magnitude of the pressure amplitude p_{an} at the antinode turns out to depend on the combination. Backhaus and Swift have carefully shaped a diameter of their looped tube to generate the acoustic wave having the pressure amplitude of 10% of a mean pressure based on an idealized lumped element equivalent.⁸ In the present work, an intense acoustic wave is obtained by using the tube with a uniform inner diameter and experimentally optimizing the combination of L_l , L_r , and R .

We measured p_{an} at the pressure antinode under the condition such that R and L_r were varied while $L_l=1.74$ m. The results are shown in Fig. 3(a). The value of p_{an} as a function of L_r shows a peak at a given R . The peak value is found to increase with decreasing R . Therefore, R was fixed at the smallest attainable value of 0.27 m. In other words, the hot end of the regenerator was located at the position as close to the resonator junction as possible.

The value of L_l was then optimized under the condition $R=0.27$ m. In Fig. 3(b), the measured p_{an} is plotted as a function of L_r under different values of L_l . Note that the data shown in Fig. 3(b) with closed circles are the same as those in Fig. 3(a) with the same symbol. As can be seen in Fig. 3(b), p_{an} at the peak can be further enhanced as L_l decreases. The largest value of p_{an} reached was 8.6 kPa, corresponding to 8.5% of the mean pressure, when $L_l=1.18$ m and $L_r=1.35$ m were chosen.

As indicated by two arrows in Fig. 3(b), the magnitude of p_{an} sharply decreases when $L_l=1.18$ m and $L_r=1.4$ –1.5 m, and $L_l=1.34$ m and $L_r=1.6$ –1.8 m. We experimentally found that two acoustic modes were simultaneously excited in the present prime mover with these two combinations. They are the quarter-wavelength and one-wavelength modes,¹⁵ in the latter of which the acoustic wave

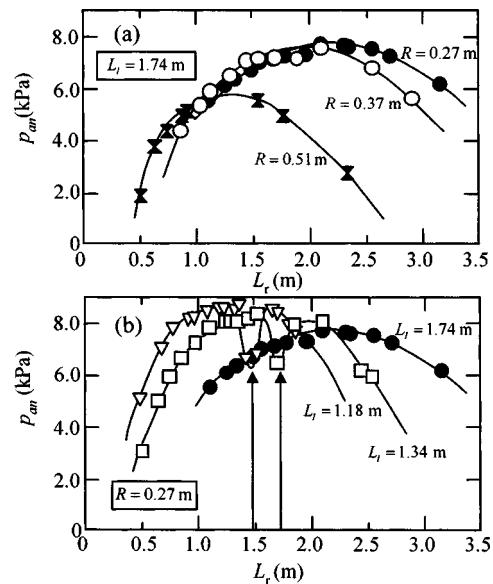


FIG. 3. The pressure amplitude p_{an} at the pressure antinode as a function of the resonator length L_r with (a) given distances R and (b) given looped tube lengths L_l . Curves are drawn to guide for the eye.

having $\lambda=L_l$ is excited. Hence, the sharp decreases of p_{an} are attributed to the competition¹⁶ between these two modes. In order to avoid an excitation of the one-wavelength mode, we finally adopted L_l , L_r , and R of 1.18, 1.04, and 0.27 m, respectively. The present prime mover thus optimized generates the spontaneous acoustic oscillation with the frequency $f=41$ Hz when Q_H is increased beyond 56 W ($T_H > 210$ °C). The pressure amplitude p_{an} becomes 8.3 kPa when Q_H reaches 210 W.

C. Simultaneous measurements of pressure and velocity

In order to reveal the mechanism of the thermoacoustic energy conversion between I and Q , we measured both velocity and pressure^{17,18} in the present prime mover. The axial velocity was measured with a laser Doppler velocimeter (LDV). In the LDV, two beams generated from a single laser source are crossed at the center of the tubes. The tracer particles (cigarette smoke) running together with an oscillating gas scatter light at the cross point of the beams. The light is detected by a photomultiplier as a burst signal. A frequency of the signal is converted to the voltage proportional to the velocity of the oscillating gas by a tracker-type processor. It should be noted that the tracker-type processor causes time delay in signal. We measured the time delay,¹⁸ and found it to be 2.7×10^{-5} s in the present experiments.

The pressure $P = p e^{i\omega t}$ was measured with a series of the pressure transducers attached on the tube wall. We experimentally found that a time delay in the pressure measurements is 0.9×10^{-6} s, which can be neglected in this experiment compared with that involved in the velocity measurement. The pressure is independent of the radial direction of the tube, because their radius ($=20$ mm) is much smaller than the wavelength λ of the acoustic wave in the present prime mover (≈ 8 m).

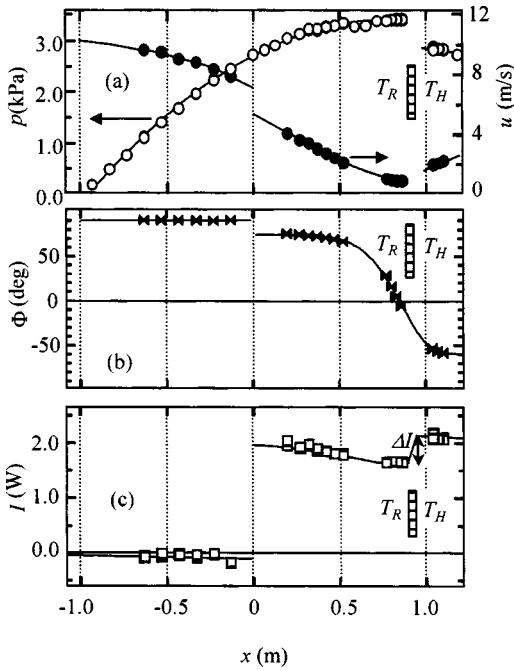


FIG. 4. Acoustic field in the thermoacoustic Stirling prime mover. The axial distribution of (a) p and u ; (b) Φ ; and (c) I . A hatched area represents the position of the regenerator and the lines are guides for the eye.

By taking the time delay in velocity measurements into account, we simultaneously measured pressure $P = p e^{i\omega t}$ and velocity $U_C = u_C e^{i(\omega t + \Phi_C)}$ along a central axis of the tube, when a heat input Q_H was 83 W. The velocity changes in a radial direction in the tube because of the presence of viscosity. Hence, the cross-sectional mean velocity $U = u e^{i(\omega t + \Phi)}$ was determined from the measured U_C by applying a laminar flow theory, which provides the relations $\Phi - \Phi_C = 0.99^\circ$ and $u/u_C = 1.02$ for the present experiment.¹⁷

D. Analysis of the measured acoustic field

The values of p , u , and Φ determined by the simultaneous measurements are plotted in Figs. 4(a) and (b) as a function of position x in the present prime mover. The resonator junction is set to be $x=0$, i.e., an origin of the coordinate shown in Fig. 2(a) and a positive direction of x is taken anticlockwise in the looped tube while it is done towards the right in the resonator.

As can be seen in Fig. 4(a), the pressure amplitude p increases whereas velocity amplitude u decreases, as x increases from -1.04 to 0.90 m. This clearly indicates that a quarter-wavelength mode was excited in the present prime mover. The phase lead Φ shown in Fig. 4(b) takes nearly 90° in the resonator ($-1.04 \leq x \leq 0$), and decreases from 85° to -60° with increasing x in the looped tube ($0 \leq x \leq 1.18$). Both values of u and Φ show discontinuities at $x=0$, where the waveguide is separated into two, so as to satisfy the laws of conservation of energy and mass.

Figure 4(c) shows the distribution of work flow I , which is calculated by inserting the data shown in Figs. 4(a) and (b) into the following equation:

$$I = A \frac{1}{2} p u \cos \Phi, \quad (4)$$

where A is the cross-sectional area of a tube. A slope of I is always negative outside the regenerator, indicating the presence of energy dissipations in the looped tube (0.34 W/m) and resonator (0.1 W/m). Note that a sign of I represents its direction. The work flow I emitted from the hot end of the regenerator ($x=0.94$) is directed toward the resonator junction ($x=1.18$) and is divided into two at the resonator junction. One is delivered to the resonator to compensate for the dissipation in it. The other runs into the looped tube in the counterclockwise direction, and is fed back into the cold end of the regenerator ($x=0.90$). The work flow reaching the cold end is amplified from 1.7 to 2.2 W in the regenerator, and the amplified work flow is output from the hot end again. The amplification of I demonstrates that the energy conversion from Q into I takes place in the regenerator. The difference of the work flow between the hot and cold ends ($\Delta I = 0.5$ W) represents the output power of the present prime mover sustaining the spontaneously induced acoustic field.

Now, we focus on the acoustic field near the regenerator. The phase lead Φ takes a pure traveling wave phase ($=0$) at $x=0.85$ m, i.e., the position close to the cold end of the regenerator. At this particular position, p and u take a maximum (3.4 kPa) and minimum (0.78 m/s), respectively. Hence, the dimensionless specific acoustic impedance z reaches the value 10 times as large as γ and is much larger than that observed by Yazaki¹⁵ in the looped tube prime mover ($z \approx 3\gamma$). The high acoustic impedance can significantly suppress viscous losses in the regenerator. The value of Φ at the center of the present regenerator is found to be about -20° , as obtained by interpolating the values at its both ends. This can be taken as evidence that the present prime mover generates the output power ΔI through the Stirling cycle because this value of Φ is near the traveling wave phase ($\Phi=0^\circ$) rather than the standing wave one ($\Phi = -90^\circ$ and 90°).

We should note two facts: (1) Φ is near the traveling wave phase and (2) its value is negative in the present regenerator. We consider that both of them are critically important in producing the output power ΔI as was discussed previously.¹² The first fact is needed to execute the Stirling cycle as mentioned above. The importance of the second one is described below. Briefly, Eq. (4) leads to the expression

$$\frac{\Delta I}{I} \approx \frac{\Delta p}{p} + \frac{\Delta u}{u} - \tan \Phi \cdot \Delta \Phi, \quad (5)$$

where Δp , Δu , and $\Delta \Phi$ represent differences in p , u , and Φ at the hot end relative to the cold one, respectively. By inserting the experimental data shown in Fig. 4 into the three terms in the right-hand side of Eq. (5), we find that $\Delta p/p \sim -0.2$, $\Delta u/u \sim 0.7$, $-\tan \Phi \cdot \Delta \Phi \sim -0.2$ across the regenerator. This means that $\Delta I/I$ is largely gained from the second term. Its positive and large value arises from the fact that the velocity node is positioned near the cold end of the regenerator because this makes its denominator a small value but the numerator large. If the velocity node with $\Phi=0$ were positioned in the regenerator, the numerator of the second term would have also become small and, thus, the second term would have been reduced as small as the first and third terms, resulting in a much smaller ΔI . Therefore, we con-

sider that the possession of a negative Φ in a regenerator is essential for producing a large ΔI while suppressing viscous losses in a thermoacoustic Stirling prime mover equipped with a looped tube and resonator.

E. Thermal efficiency of the thermoacoustic prime mover

The present thermoacoustic Stirling prime mover turns out to have the output power ΔI of 0.5 W when $Q_H = 86$ W. Its thermal efficiency is about 0.6%. This is much smaller than that reported by Backhaus and Swift (30%). The low efficiency may be attributed to the use of atmospheric air as a working gas in the present prime mover. The use of atmospheric air is required in the present work to measure the acoustic field with LDV. On the other hand, Backhaus and Swift used helium gas with a mean pressure P_m of 3 MPa. Based on the performance of the present prime mover, we consider below what efficiency a thermoacoustic Stirling prime mover of this type will gain when such a highly pressurized gas is employed.

The work flow at the pressure antinode, where $\Phi = 0$, is obviously given from Eq. (4) as

$$I = \frac{AP_m c}{2z} \left(\frac{p}{P_m} \right)^2, \quad (6)$$

where $\cos \Phi = 1$ and $z = (p/P_m)/(u/c)$ are used. In the case of the Backhaus and Swift thermoacoustic prime mover, for example, A is 6.2×10^{-3} m², P_m is 3 MPa, and c is 1.0 km/s. They obtain $p/P_m = 0.1$ when the input heat power is 4.0 kW, and estimate z at 15–30 γ ($\gamma \sim 1.66$ for helium).⁸ Hence, the work flow at the pressure antinode would become 3.8–1.9 kW. Assuming that this amount of the work flow running into the regenerator is amplified by the ratio $\Delta I/I = 0.3$ in the same way as that in the present prime mover, we can evaluate the output power to be 1.1–0.6 kW. Hence, the thermal efficiency of their prime mover would become 25%–15%. The efficiency thus estimated would refer to only a possible minimum value for their prime mover, because the temperature ratio $\eta = (T_H - T_C)/T_C$ of 2.3 in their prime mover is higher than that in the present one ($\eta = 0.8$). All the analysis above indicates that an extremely high efficiency achieved by the Backhaus and Swift is reasonably understood from the extension of the present results.

F. Visualization of an acoustic streaming

We discuss in this subsection a visualization of the gas motions from the Lagrangian point of view, which allows us to measure a secondary flow induced in the present prime mover. The motivation for this measurement is that it has been pointed out that the net of the secondary flow carries heat away from the hot heat exchanger on the regenerator and generates an unwanted heat leak, resulting in a decrease in an efficiency.^{8,19} A sheet-like plane light of a 400-mW argon-ion laser was passed through the axis of the looped tube. Tracer particles of 20 μ m in diameter were introduced within the tube, where spontaneous gas oscillations were excited with $Q_H = 86$ W, i.e., the same condition as that employed in the pressure and velocity measurements.

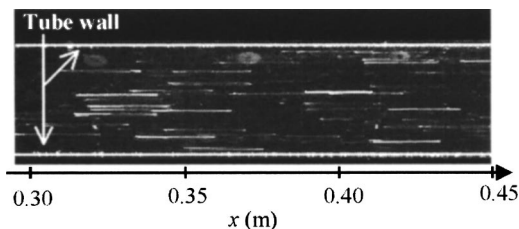


FIG. 5. Visualization of the streaming. Bright lines represent traces of the moving tracer particles.

Figure 5 shows a typical photograph taken in the region over $x = 0.30$ to 0.45 m. The traces of the particles are seen as horizontal bright lines in Fig. 5. This is because the shutter speed was slower than the inverse of the oscillating frequency ($1/41$ s) and the velocity in the tube is uniaxial. The length of the line, therefore, represents the peak-to-peak displacement of the tracer particle, and is found to be 26 mm at $x = 0.35$ m. This agrees well with the peak-to-peak displacement estimated from the velocity measurements shown in Fig. 4(a).

We found that bright lines moved slowly with the dc velocity U_0 along the tube axis. This indicates the existence of a secondary flow in the present prime mover. It turned out that U_0 depends on the radial coordinate. At the center of the tube, U_0 was about 34 mm/s and its flow was always directed from right to left. This is opposite to the direction of I . Near the tube wall, U_0 was faster than that at the center. Its direction was reversed and became the same as that of I . However, the net flow rate of the secondary flow and its direction could not be experimentally observed in the present prime mover. Therefore, it was experimentally unclear whether the secondary flow significantly reduced the efficiency of the present prime mover or not.

III. CONSTRUCTION OF A COOLER DRIVEN BY THE THERMOACOUSTIC STIRLING PRIME MOVER

A. Thermoacoustic cooling effect

This section describes the construction and performance of a cooler driven by the present thermoacoustic Stirling prime mover. The present prime mover generates the output power ΔI through the Stirling cycle. By using this ΔI as a source of power, we produce a thermoacoustic cooling effect¹⁵ without moving parts. A second regenerator, which acts as a thermoacoustic heat pump, was inserted into the present thermoacoustic prime mover.

The measured acoustic field allowed us to locate precisely a right position for the installation of the second regenerator. The position is $x = 0.85$ m, because the acoustic impedance z becomes the maximum (10γ) and Φ takes exactly zero there. The maximum acoustic impedance can significantly reduce viscous losses in the second regenerator to a minimum level. The traveling wave phase can cause a thermoacoustic cooling effect through the reversed Stirling cycle as explained below. As can be seen Fig. 1(a), a gas parcel having $\Phi = 0$ in the second regenerator will experience the following cycle: (1) pressure of the gas parcel is increased near one end of its travel and then, the gas parcel releases heat to the wall of the second regenerator, since the tempera-

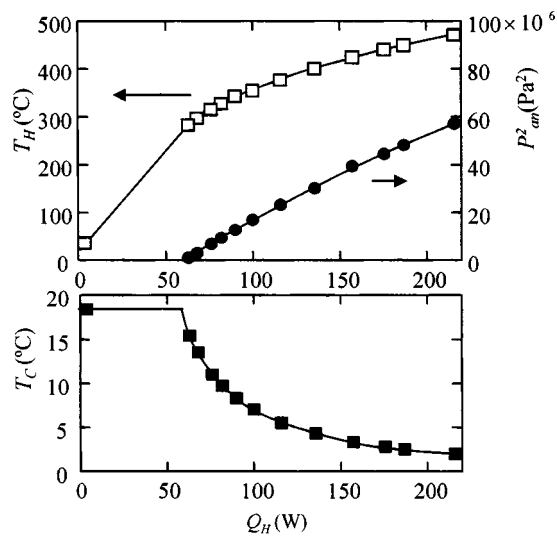


FIG. 6. Performance of the thermoacoustic Stirling cooler with the use of atmospheric air. Temperatures T_H at the hot end of the regenerator, in which the output power is generated, and T_C at the cold end of the second regenerator, in which the heat pump effect is operated, and square of pressure amplitude p_{an}^2 are plotted as a function of input power Q_H . The lines are guides for the eye.

ture of the gas parcel is kept equal to that of the wall through the thermal contact between them; (2) the gas parcel moves toward the other end; (3) where its pressure is decreased and then, it receives heat from the wall, and (4) it moves back to the first position. By repeating this cycle, a heat flow can be pumped from one end to the other of the second regenerator in the opposite direction to I , resulting in the generation of a temperature gradient along it.

B. Construction of a thermoacoustic Stirling cooler

Figure 2(b) shows the schematic illustration of a ceramic honeycomb used as the second regenerator. The regenerator of 80 mm in length has many square pores with the cross section $0.6 \times 0.6 \text{ mm}^2$. Two heat exchangers are placed on both sides of the regenerator. One is cooled by water to keep it at T_R . The other is exposed to surrounding air and its temperature T_C is measured by a thermocouple. The second regenerator is located in the position over $x=0.77$ to 0.85 m in the present prime mover.

We tested the performance of the cooler by gradually increasing Q_H . Figures 6(a) and (b) shows the measured T_H , T_C , and p_{an}^2 as a function of Q_H . The temperature T_H monotonically increases with increasing Q_H , but p_{an}^2 and T_C remain unchanged at 0 and room temperature of 18°C as long as $Q_H \leq 63 \text{ W}$, respectively, because of the absence of gas oscillations. When Q_H exceeds Q_{crit} of 63 W , the gas parcels begin to oscillate. Now, p_{an}^2 becomes finite and T_C begins to decrease from room temperature. This proves that the heat flow was indeed pumped across the second regenerator from its cold heat exchanger (T_C) to the room-temperature one (T_R) by thermoacoustically generated gas oscillations. We measured the pressure along the tube and found that the position of the pressure antinode, where $\Phi = 0$, remained unchanged upon the installation of the second regenerator. Therefore, the reversed Stirling cycle to pump

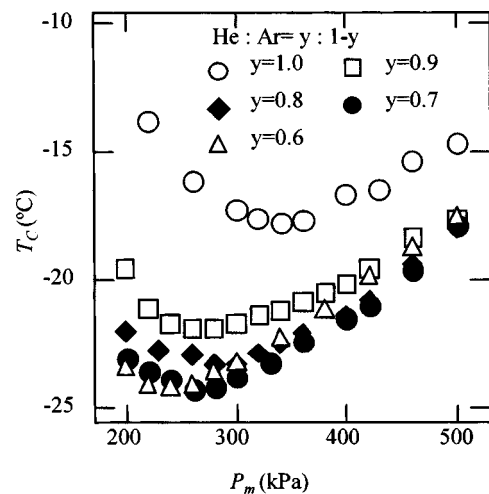


FIG. 7. Temperature T_C of the cold end of the second regenerator as a function of P_m , for input power $Q_H=210 \text{ W}$.

heat is executed in the second regenerator. With increasing Q_H , p_{an}^2 increases and T_C decreases. When Q_H is increased to 210 W , p_{an} reaches 7.5 kPa and T_C drops to the lowest temperature of 2°C .

C. Cooler filled with pressurized gas

In order to further enhance the cooling performance, we modified the cooler in the way discussed below. The glass looped tube and resonator are replaced by stainless-steel tubes with 40 mm inner diameter. Pressurized helium gas with mean pressure of $P_m=220\text{--}500 \text{ kPa}$ is employed as working gas in place of atmospheric air. The values of L_l , L_r , and R are adjusted to be 1.04 , 1.40 , and 0.20 m , respectively. In the high-pressure cooler thus constructed, the frequency f of the spontaneous gas oscillations turned out to be 118 Hz .

Under the condition $Q_H=210 \text{ W}$, we measured T_C in the high-pressure thermoacoustic cooler as a function of P_m . The measured T_C , as shown in Fig. 7 by open circles, reaches -13.8°C at $P_m=220 \text{ kPa}$ and is further decreased with increasing P_m up to 350 kPa . The value of T_C reaches the lowest value of -17.8°C at $P_m=350 \text{ kPa}$ but is increased with further increase in P_m beyond 350 kPa .

The existence of the minimum on the T_C - P_m curve can be explained by using the relations

$$\delta_v \propto (P_m \omega)^{-1/2}, \quad (7)$$

and

$$\delta_t = \delta_t \sigma^{1/2}, \quad (8)$$

where σ is Prandtl number, and δ_v and δ_t are the viscous and thermal penetration depths,¹⁴ respectively. The viscous penetration depth δ_v can be decreased by increasing P_m through Eq. (7), resulting in the suppression of viscous losses generated in the two regenerators. However, δ_t is also decreased by increasing P_m through Eq. (8). A decreasing δ_t will cause the loss of a good thermal contact between a gas parcel and the wall in the regenerators. Since a good thermal contact is indispensable for the Stirling prime mover and cooler, an increase in P_m beyond some critical value will reduce the

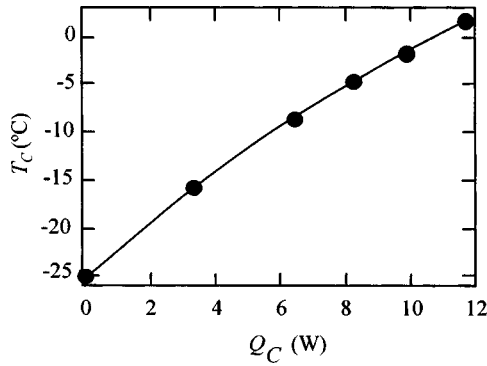


FIG. 8. Cooling power of the thermoacoustic Stirling cooler. Temperature T_C of the cold end of the second regenerator is plotted as a function of the load Q_C , when an input power $Q_H=210$ W. The line is a guide for the eye.

performance of the cooler as shown in Fig. 7.

We tried to decrease T_C further. Equation (8) indicates that, if σ can be decreased, δ_v is decreased, resulting in a decrease of viscous losses. Since σ can be decreased by using a mixture of helium and argon,²⁰ we employed it as a working gas. While adding argon to helium, we measured the temperature T_C with $Q_H=210$ W.

The value of T_C is shown in Fig. 7 as a function of P_m at a given ratio of helium to argon. The ratio was estimated from the measured frequency f_{mix} of the spontaneous gas oscillation for the mixture and the equation,

$$\frac{f_{\text{He}}}{f_{\text{mix}}} = \sqrt{\frac{(1-y)N_{\text{Ar}} + yN_{\text{He}}}{N_{\text{He}}}}, \quad (9)$$

where f_{He} ($=118$ Hz) is the frequency for pure helium in the present cooler and N_{He} and N_{Ar} are the molar mass of helium and argon, respectively, and y is a mole fraction of helium. The T_C - P_m curves with the mixture fall consistently lower than that with pure helium in the region $200 \leq P_m \leq 500$ kPa. The mixture at a given ratio also takes an optimum value of P_m in the same reason as that with pure helium. The optimum P_m of the mixture is lower than that of pure helium. This is attributed to the fact that the mixture can reduce viscous losses while keeping a good thermal contact at low P_m compared with helium. As can be seen in Fig. 7, when y was 0.7 and P_m was the optimum value of 260 kPa, we obtained the lowest temperature T_C of -25 °C, which was lower by 47 °C than room temperature T_R (≈ 22 °C).

Finally, we demonstrate the cooling power of the present cooler with the choice of the optimized mixture gas, where $y=0.7$ and $P_m=260$ kPa. A resistance heater was wound around the cold heat exchanger on the second regenerator and the cooling power was measured under the condition $Q_H=210$ W. In Fig. 8, T_C is plotted as a function of the heat load Q_C supplied to the heater. As Q_C increases to 12 W, T_C raises from -25 to 2 °C. The thermal efficiency of the cooler defined as Q_C/Q_H turns out to be 5% at 0 °C.

IV. SUMMARY

We have measured the acoustic field in the thermoacoustic prime mover having the looped tube and resonator by simultaneous measurements of pressure P and cross-sectional mean velocity U . The acoustic field thus observed

enabled us to prove that the thermoacoustic Stirling prime mover executes the thermodynamic cycle by using an acoustic wave having a high acoustic impedance and a negative phase lead Φ . We consider that a negative Φ plays a key role to increase the efficiency of a thermoacoustic prime mover having a looped tube and resonator. Moreover, based on these experimental results, we succeeded in constructing a Stirling cooler driven by the present thermoacoustic prime mover. The cooler generated a temperature of -25 °C and had a cooling power Q_C of 11 W at 0 °C with an input power Q_H of 210 W.

The thermoacoustic prime mover and cooler have a potential to become an efficient device, because the mutual conversions between Q and I are executed through the Stirling cycle which has an inherent reversibility. They are very inexpensive to maintain and to construct it, and produce neither waste gas nor require chlorofluorocarbon. We consider that a thermoacoustic prime mover and cooler will become a new technology to use a waste and solar heat with a high efficiency and low cost.

¹G. W. Swift, "Thermoacoustic engines and refrigerators," *Phys. Today* **48**, 22–28 (1995); "Thermoacoustic engines" *J. Acoust. Soc. Am.* **84**, 1145–1180 (1988).

²A. Tominaga, "Thermodynamic aspects of thermoacoustic theory," *Cryogenics* **35**, 427–440 (1995).

³J. C. Wheatley, T. Hofer, G. W. Swift, and A. Migliore, "Experiments with an intrinsically irreversible acoustic heat engine," *Phys. Rev. Lett.* **50**, 499–502 (1983); "An intrinsically irreversible thermoacoustic heat engine," *J. Acoust. Soc. Am.* **74**, 153–170 (1983); "Understanding some simple phenomena in thermoacoustics with applications to acoustical heat engines," *Am. J. Phys.* **53**, 147–162 (1985).

⁴Work flow I is defined as $I=A \cdot \langle PU_r \rangle$ and heat flow Q is defined as $Q=A \cdot \rho_m \cdot T_m \cdot \langle SU_r \rangle$, where the bars and angular brackets indicates the time and radial averages, and A is cross-sectional area, ρ_m , T_m , S , and U_r are mean mass density, mean temperature, entropy per unit mass, and axial velocity, respectively.

⁵A. A. Atchley and F. Kuo, "Stability curves for a thermoacoustic prime mover," *J. Acoust. Soc. Am.* **95**, 1401–1404 (1994).

⁶A. A. Atchley, "Analysis of the initial buildup of oscillations in a thermoacoustic prime mover," *J. Acoust. Soc. Am.* **95**, 1661–1664 (1994).

⁷R. Radebaugh, K. M. McDermott, G. W. Swift, and R. A. Martin, "Development of a thermoacoustically driven orifice pulse tube refrigerator," in *Proceedings of the Interagency Meeting on Cryocoolers*, p. 205. 24, October 1990, Plymouth MA.

⁸S. Backhaus and G. W. Swift, "A thermoacoustic Stirling heat engine," *Nature (London)* **399**, 335–338 (1999); "A thermoacoustic-Stirling heat engine: Detailed study," *J. Acoust. Soc. Am.* **107**, 3148–3166 (2000).

⁹P. H. Ceperley, "A pistonless Stirling engine—traveling wave heat engine," *J. Acoust. Soc. Am.* **66**, 1508–1513 (1979).

¹⁰S. Garrett, "Reinventing the engine," *Nature (London)* **399**, 303–305 (1999).

¹¹T. Yazaki, A. Iwata, T. Maekawa, and A. Tominaga, "Traveling wave thermoacoustic engine in a looped tube," *Phys. Rev. Lett.* **81**, 3128–3131 (1998).

¹²Y. Ueda, T. Biwa, T. Yazaki, and U. Mizutani, "Acoustic field in a thermoacoustic Stirling engine having a looped tube and resonator," *Appl. Phys. Lett.* **81**, 5252–5254 (2002).

¹³The hydraulic radius is the ratio of gas volume to gas–solid contact area.

¹⁴The thermal penetration depth δ_t is defined as $\sqrt{2\alpha/\omega}$, where α is a thermal diffusivity defined by using thermal conductivity κ , isobaric heat capacity c_p , and mean density ρ_m as $\kappa/(c_p\rho_m)$.

¹⁵T. Yazaki, T. Biwa, and A. Tominaga, "A pistonless Stirling cooler," *Appl. Phys. Lett.* **80**, 157–159 (2002).

- ¹⁶T. Biwa, Y. Ueda, T. Yazaki, and U. Mizutani, "Thermodynamical mode selection rule observed in thermoacoustic oscillations," *Europhys. Lett.* **60**, 363–368 (2002).
- ¹⁷T. Yazaki and A. Tominaga, "Measurement of sound generation in thermoacoustic oscillations," *Proc. R. Soc. London, Ser. A* **454**, 2113–2122 (1998).
- ¹⁸T. Biwa, Y. Ueda, T. Yazaki, and U. Mizutani, "Work flow measurements in a thermoacoustic engine," *Cryogenics* **41**, 305–310 (2001).
- ¹⁹S. Backhaus and G. W. Swift, "An acoustic streaming instability in thermoacoustic devices utilizing jet pumps," *J. Acoust. Soc. Am.* **113**, 1317–1324 (2003).
- ²⁰J. R. Belcher, W. V. Slaton, R. Raspet, H. E. Bass, and J. Lightfoot, "Working gases in thermoacoustic engines," *J. Acoust. Soc. Am.* **105**, 2677–2684 (1999).